Electronic structure of CoO, Li-doped CoO, and $LiCoO_2$

J. van Elp, J. L. Wieland, H. Eskes, P. Kuiper, and G. A. Sawatzky
Department of Solid State and Applied Physics, Materials Science Centre, University of Groningen, Nijenborgh 18, NL-9747AG Groningen, The Netherlands

F. M. F. de Groot
Research Institute for Materials, University of Nijmegen, Toernooiveld, NL-6525 ED Nijmegen, The Netherlands

T. S. Turner
Science and Engineering Research Council, Daresbury Laboratory, Daresbury Warrington WA4 4AD, United Kingdom

(Received 27 November 1990; revised manuscript received 3 June 1991)

The electronic structure of $Li_xCo_{1-x}O$ ($0.01 \leq x \leq 0.2$), $LiCoO_2$, and Co_3O_4(1% Li) has been investigated using x-ray photoemission spectroscopy (XPS), bremsstrahlung isochromat spectroscopy (BIS), and x-ray-absorption spectroscopy. The experimental results are compared with model cluster calculations. We find that the CoO band gap is of an intermediate character, between Mott-Hubbard-like and charge-transfer-like. The first ionization state of CoO is therefore of strongly mixed Co $3d$ and O $2p$ character. Its local symmetry corresponds to $^3T_{1g}$, similar to an intermediate-spin Co^{3+} state. For $x \leq 0.2$ the local Co electronic structure is similar to that of CoO. However, $LiCoO_2$ has a strongly reduced Co-O interatomic distance, resulting in a ligand field strong enough to stabilize a Co^{3+} low-spin ground state. $LiCoO_2$ is an insulator with a gap of 2.7 eV. From a comparison of the XPS and BIS CoO spectra to the cluster calculations, we find values for U (=5.3 eV), Δ (=5.5 eV), and $(pd\sigma)$ (=1.3 eV).

INTRODUCTION

The late-transition-metal oxides have been the subject of intense experimental and theoretical investigations since the discovery that these oxides are insulators,[1] while one-electron band theory[2,3] predicts them to be metallic. The discovery of the high-T_c superconducting materials[4] has renewed the interest in the electronic structure of the late-transition-metal oxides. The insulating behavior of these oxides is thought to be caused by the strong correlation effects that are also responsible for the breakdown of the one-electron picture. A gap is opened that suppresses the high-energy (U) polarity fluctuations like $d_i^n d_j^n \rightarrow d_i^{n+1} d_j^{n-1}$. The absence of these charge fluctuations gives rise to the famous Mott-Hubbard picture[5,6] of the insulators with an energy U between the first ionization state and first affinity state. Although it describes the insulating nature of the late-transition-metal oxides well, it cannot easily describe why many sulfides are metallic or the dependence of the band gap on electron negativity in general.[7] To understand this we also have to take the charge-transfer energy Δ, involved in $d^n \rightarrow d^{n+1}\underline{L}$, into account. Here $\underline{L}$ denotes a hole in the anion (oxygen) p band. Δ is directly related to the electronegativity of the anion.

Up to a few years ago the gap in NiO was thought to be a d-d gap. Fujimori and Minami[8] showed that the first ionization state in NiO is of mainly $d^8\underline{L}$ character, making it a charge-transfer insulator with a ligand p to metal d gap. The actual gap of NiO is shown in an x-ray photoemission spectroscopy (XPS)–bremsstrahlung isochromat spectroscopy (BIS) experiment to be about 4 eV.[9] Also, CuO (Ref. 10) and the parent compounds of the Cu-based high-T_c oxides[11,12] are shown to be charge-transfer insulaters.

In the past there has been a lot of research on the Li-doped transition-metal oxides. The magnetic susceptibility experiments for $Li_xNi_{1-x}O$ (Ref. 13) and $Li_xCo_{1-x}O$ (Ref. 14) were explained by assuming the presence of trivalent Ni and Co both in the low-spin ($S=\frac{1}{2}$ and 0, respectively) state. Conductivity, Seebeck-, and Hall-effect experiments have been done; they showed that $Li_xCo_{1-x}O$ does not have the features of small-polaron conduction.[15,16] The $LiCoO_2$ end member has been investigated for use in batteries.[17] They found that the Li could be almost completely removed electrochemically, leaving about 7% Li at room temperature in the electrolyte stable structure.

In an oxygen 1s (K edge) x-ray-absorption spectroscopy (XAS) study[18] it is shown that for $Li_xNi_{1-x}O$ the holes are mainly on the oxygen and are localized around the Li impurity, making it a semiconductor. The antiferromagnetic coupling of the oxygen-hole spin around the Li with the Ni spin results in a static moment that looks like low-spin Ni^{3+} ($S=\frac{1}{2}$). In a BIS study of $Li_xNi_{1-x}O$ (Ref. 19) one sees that the Li-induced impurity states are spread over a wide energy range in the NiO gap, leaving a small gap (~0.5 eV) in the heavily doped ones.

The first ionization state of CoO is of considerable importance when considering the location of the charge compensating holes in Li-doped CoO. In the extreme case of $U > \Delta$ the compensating holes would be in O $2p$ states, whereas for $U < \Delta$ they would lead to Co^{3+} states.

Estimated values of U and Δ in transition-metal monoxides yield for CoO $U \sim \Delta$,[20,21] placing CoO in the intermediate region of the Zaanen-Sawatzky-Allen (ZSA) diagram.[22] However, if we look at the existing cobalt oxides, we have, besides divalent Co in CoO, also Co_3O_4 and Co_2O_3, in which Co is also in the formal trivalent state.

In this paper we present x-ray photoemission, bremsstrahlung isochromat spectroscopy, and x-ray-absorption spectroscopy data on $Li_xCo_{1-x}O$, $LiCoO_2$, and Co_3O_4. Although XPS measurements[23–26] and ultraviolet photoemission spectroscopy (UPS) measurements[26–29] on some of these oxides have been reported, there is no published work on the unoccupied electron states as measured with BIS and oxygen 1 s (K edge) and cobalt $2p$ ($L_{2,3}$ edges) XAS. The spectral distributions measured with the various spectroscopies are compared to model Hamiltonian cluster calculations, from which we extract model Hamiltonian parameters for CoO and the nature of the first ionization and electron affinity states. One of the most important conclusions is that although the holes initially go into the O $2p$ band with Li doping, the end-member $LiCoO_2$ contains low-spin Co^{3+}.

SAMPLE PREPARATION AND EXPERIMENTAL DETAILS

The $Li_xCo_{1-x}O$ system is a high-temperature phase[14] with possible Li substitution up to $x=0.2$ followed by a miscibility gap up to $LiCoO_2$ (Table I). The $Li_xCo_{1-x}O$ samples have the NaCl structure with a decreasing lattice parameter as a function of increasing Li content. The structure of $LiCoO_2$ is comparable to $LiVO_2$, $LiCrO_2$, and $LiNiO_2$. It is a NaCl superstructure with metal ordering in the (111) cubic metal layers, which are alternatively occupied by Li and Co atoms.[14] The structure is fully ordered according to neutron-powder-diffraction data[30] and the CoO_6 octahedra are compressed, whereas the LiO_6 octahedra are elongated.

The $Li_xCo_{1-x}O$ samples are made by grinding together the proper proportions of Li_2CO_3 and CoO or Co_3O_4. If we start with CoO, the first step is to heat the pelletized powders under a flow of dry oxygen at 950 °C for 16 h. We then get a Li-substituted Co_3O_4 spinel structure. The next step is to regrind and pelletize them again followed by heating at 1050 °C in a pure-argon atmosphere for 24 h. This temperature is sufficient for the transition to the monoxide structure. The transformation from the high-temperature phase to the lower-temperature two-phase mixture is slow enough that by fast cooling from 1050 °C the high-temperature phase can be retained. If we start with Co_3O_4, the first step can be omitted, but regrinding and heating again gives mechanically better samples.

All the transformations and phases were checked by x-ray diffraction. The x-ray-diffraction data showed a homogeneous material, but the method is not sensitive to the presence of unreacted lithium oxide. It showed less than 1% $LiCoO_2$ present in the $Li_xCo_{1-x}O$ samples, and the amount of Li put in was consistent with the lattice-parameter variation with x.[14] A wet chemical analysis was also used to determine the Li content and confirmed the x-ray-diffraction results.

The $LiCoO_2$ samples are made by heating the proper amounts of Li_2CO_3 and CoO or Co_3O_4 in dry oxygen at 950 °C. X-ray diffraction shows homogeneous samples of single phase. In the XPS, BIS, and resonant photoemission measurements, we used a mechanically stronger sample, which was also heated for 72 h in argon. Here we found about 1% of Co_3O_4 present, probably because of Li volatilization.

The Co_3O_4 samples were made by simply heating CoO or Co_3O_4 in dry oxygen at 1050 °C. In the BIS and XPS experiments we used at 1%-Li-doped sample to increase the conductivity. The Li substitution can go up to 10% in Co_3O_4.[31]

The XPS and BIS measurements were done using a modified Kratos 200 spectrometer, with a background pressure in the low 10^{-10}-Torr range. The XPS source was the unmonochromated Mg $K\alpha$ line (1253.6 eV). For BIS we use the Al $K\alpha$ (1486.6 eV) monochromater for photon detection and a home-built type of Pierce electron gun, capable of giving electron currents of approximately 200 μA. The instrumental broadening is estimated to be 1.0 eV for XPS and 0.8 eV for BIS. All the ceramics measured were scraped *in situ* with a diamond file.

BIS measurements can be severely plagued by charging effects because the electron current is quite high compared to XPS. The charging effects we encountered could be taken care of by heating the samples up to a few 100 °C. All the BIS measurements reported here were

TABLE I. Crystallographic parameters. [References: A. F. Wells, *Structural Inorganic Chemistry* (Clarendon, Oxford, 1984); Refs. 14, 30, and 44.]

	CoO	$LiCoO_2$	Co_3O_4	NiO	CuO
Lattice parameter	cubic $a=4.26$ Å	hexagonal $a=2.815$ Å $c=14.05$ Å	cubic, spinel $a=8.065$ Å $\mu=0.3881$	cubic $a=4.18$ Å	Monoclinic $a=4.68$ Å $b=3.42$ Å $c=5.13$ Å $\beta=99.54°$
Shortest m-O distance	2.13 Å	1.921 Å	1.916 Å(o) 1.929 Å(t)	2.09 Å	1.95 Å

taken in several scans that were added afterwards. The samples were checked before and after the BIS measurements with XPS. At a temperature of 300 °C the surface of Co_3O_4(1% Li) changed to CoO; this could be overcome by taking short scans with scraping in between.

The resonant photoemission experiments on $LiCoO_2$ were carried out at SRS in Daresbury using the TGM6A beamline. We used an ADES-400 spectrometer equipped with a 127° hemispherical analyzer. The analyzer resolution used is 0.1 eV. The synchrotron energy ranges from 20 to 90 eV using two different gratings (710, 1800 lines/mm). The monochromator resolution ranges from 0.1 to 0.3 eV. The base pressure in the measurement and preparation chamber was in the low 10^{-10} mbar. The sample was scraped *in situ* using a diamond file.

The O 1*s* XAS measurements were done at the Berlin synchrotron BESSY with a SX700 monochromator.[32] We operated with an exit slit of 10 μm, giving a resolution of about 500 meV at the oxygen 1*s* absorption energy. The spectra were taken in the total electron yield method, which probes a layer several hundreds of angstroms deep. The total yield was divided by the storage ring current recorded simultaneously. The absolute energy scale was determined by measuring a Cr metal edge in first order and a Co metal edge in first and second order. The energy positions were within 0.1 eV of those measured with high-energy electron loss spectra of Fink *et al.*[33] The samples were scraped in 10^{-9}-Torr vacuum with an alumina file. The Co 2*p* XAS measurements were done on the Dragon monochromator[34] in Brookhaven. The experimental details will be published elsewhere.[35]

EXPERIMENTAL RESULTS

We start with a comparison of the spectra of the $Li_xCo_{1-x}O$ for $x \leq 0.2$, $LiCoO_2$, and Co_3O_4. In Fig. 1 the XPS data in the O 1*s* binding-energy region are shown. As has been recently shown from cluster calculations using Cu_2O_7 and Cu_2O_8 clusters, satellite structure in the O 1*s* spectrum is very weak and spread out over a broad energy range even in the doped samples.[36] The shoulder observed at about 531 eV is therefore most likely due to some remaining small amount of contamination of water, hydroxide, or defect structure at the grain boundaries. The low intensity of the shoulder, however, indicates quite clean and reliable samples. The binding energy of the main line given in Table II is seen to be nearly independent of sample composition, indicating only small shifts if any in the Fermi level.

In Fig. 2 we show the Co $2p^{3/2}$ XPS core lines. These consist for $Li_xCo_{1-x}O$ ($x \leq 0.2$) of a main line at about 780 eV and a strong satellite at about 6-eV higher binding energy. The binding energies are tabulated in Table II. For $x \leq 0.2$ the spectra are almost identical. The satellite intensity hardly changes, and also the widths of the lines stay nearly constant. This indicates that Li substitution does not strongly alter the local electronic structure of Co for $x \leq 0.2$. However, the spectrum of $LiCoO_2$ is dramatically different. The main line has sharpened up and the satellite has changed into a low-intensity broad structure. This spectrum is also quite different from those of the Co dihalides,[37,38] indicating a local electronic structure quite different from that expected for Co^{2+}. The spectrum is similar to the one reported by Oku.[25] Bongers[39] found that Co in $LiCoO_2$ is diamagnetic and explained this by assuming Co^{3+} to be in low spin ($S=0$). The Co_3O_4 spectrum is in between that of $LiCoO_2$ and CoO, which would agree with the nominal valency of Co,Co^{3+} for the two octahedral positions and Co^{2+} for the tetrahedral position.

These same qualitative trends are seen in the high-resolution Co $2p^{3/2}$ XAS edges measured on the Dragon

TABLE II. Core-level binding energies relative to the Fermi level and gaps.

	O 1*s* (eV)	Co $2p^{3/2}$ (eV)	Gap (eV)
$Li_xCo_{1-x}O$ with			
$x=0.01$	529.4	779.8	2.5±0.3
$x=0.1$	529.3	779.8	2.4±0.3
$x=0.2$	529.3	779.8	2.0±0.3
$x=0.5$	529.2	779.5	2.7±0.3
Co_3O_4(1% Li)	529.2	779.4	1.6±0.3

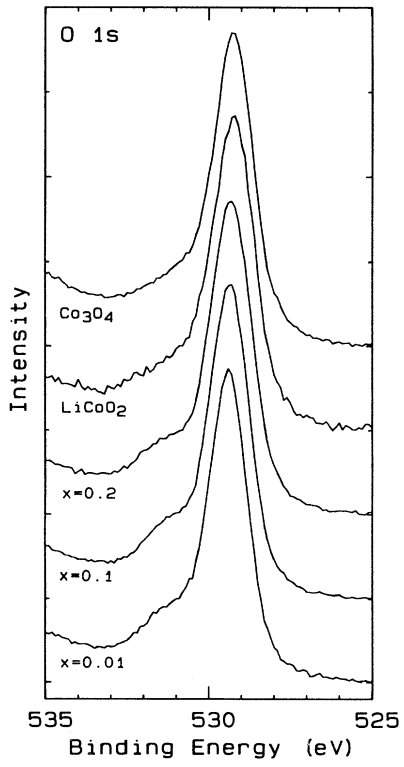

FIG. 1. O 1*s* XPS spectra of $Li_xCo_{1-x}O$, $LiCoO_2$, and Co_3O_4. The shoulder observed at high binding energy is most likely due to a small amount of water, hydroxide, or defect structure present at the grain boundaries.

monochromator in Brookhaven.[35] These edges shown in Fig. 3 exhibit a rich multiplet structure, which is characteristic for Co^{2+} in O_h symmetry, and a crystal-field splitting $10Dq$ of ~ 1 eV for $Li_xCo_{1-x}O$ ($x \leq 0.2$) and for low-spin Co^{3+} in $LiCoO_2$ (see Fig. 14 in Ref. 40). The low-intensity shoulder at low energies for $LiCoO_2$ is due to a small amount of Co_3O_4 contamination. These spectra again show that the local electronic structure changes little for $x \leq 0.2$, with a radical change for $x = 0.5$ or $LiCoO_2$. Although not shown in Fig. 3, XAS shows little if any satellite intensity, quite different from XPS, because the extra $3d$ electron in the $2p$-$3d$ transition of XAS almost perfectly screens the core-hole potential.

A somewhat different situation is encountered in the O $1s$ absorption edges shown in Fig. 4. Here the structue above about 535 eV is due to O $1s$ transitions to higher-lying bands of Co $4s,4p$ and O $3p$ character, the first two of which have considerable O $2p$ character mixed in.[41] The structure between 530 and 535 eV is due to transition to the Co $3d$ states and Li-induced hole states. These unoccupied Co $3d$ states can be reached by O $1s$ absorption because of the O $2p$ hole character in the ground state due to hybridization, as described by Kuiper *et al.*[18] for NiO. The double-peaked structure in CoO is a result of the multiplet splitting of the Co (d^8) states, as will be discussed below. In the simplest of crystal-field pictures, the ground state of Co (d^7) would be $((t_{2g}\uparrow)^3(e_g\uparrow)^2(t_{2g}\downarrow)^2)$, which contains t_{2g} and e_g holes of the same spin, and split by $10Dq$. We then expect two peaks split by the crystal field ($10Dq$), as discussed by de Groot *et al.*[42] A more exact calculation gives actually four peaks, as discussed below. Upon Li substitution the lowest-energy peak that would correspond to filling a t_{2g} hole in the simple picture grows gradually until in $LiCoO_2$ this peak dominates the pre-edge. This is quite different from the O $1s$ edge in $Li_xNi_{1-x}O$ (Ref. 18), where a well-separated pre-edge peak appears with Li substitution. Also, this behavior in the O $1s$ edge is quite different from that of the Co $2p$ edge and the Co $2p$ and O $1s$ XPS, where little happens for $x \leq 0.2$. We will discuss this feature below.

The valence-band XPS and conduction-band BIS structures are shown in Fig. 5. Because of the high photon energies in both cases, the structures are dominated by Co $3d$ electron removal and addition spectral weights. We find the very broad distribution of valence-band states spread out over an energy scale of 10 eV or more. One-electron band theory yields a $3d$ partial density of states strongly peaked close to E_f and a small tail up to about

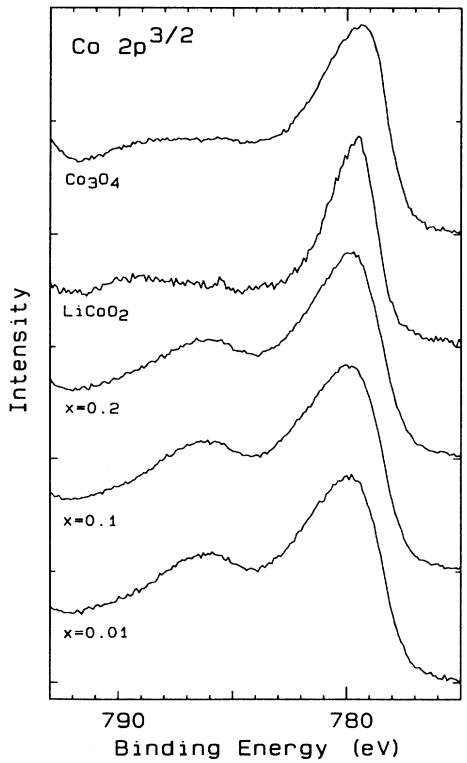

FIG. 2. Co $2p^{3/2}$ core line XPS spectra of $Li_xCo_{1-x}O$, $LiCoO_2$, and Co_3O_4.

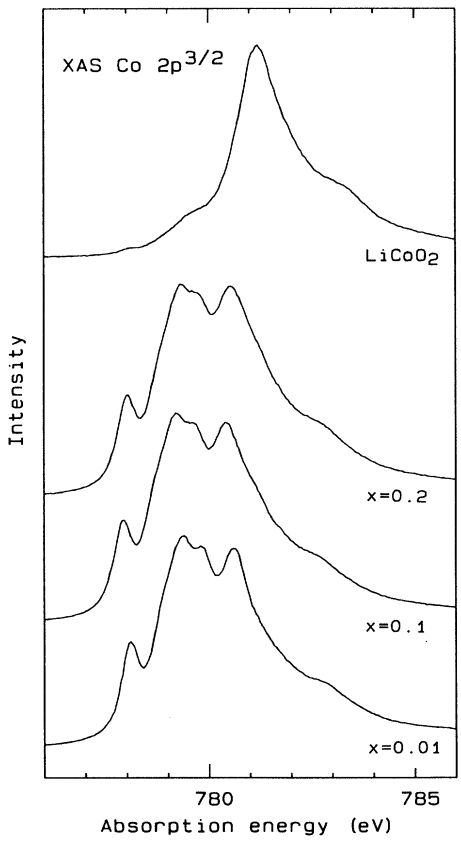

FIG. 3. High-resolution Co $2p^{3/2}$ XAS spectra of $Li_xCo_{1-x}O$ and $LiCoO_2$. The absorption at about 779 eV in $LiCoO_2$ is due to some Co_3O_4 contamination.

6-eV binding energy, as shown in Fig. 6.[43] The energy range observed experimentally is a direct result of large electron-electron interactions, yielding a large energy spread of the different electron removal states (d^6, $d^7\underline{L}$, $d^8\underline{L}^2$, etc.), each with its own multiplet spread. Also in the spectra there is little change with x for $x \leq 0.2$ and a quite dramatic change for $LiCoO_2$, in which the first peak sharpens up and the satellite structure changes drastically. For $x \leq 0.2$ the Fermi level stays pinned at 0.7 eV above the top of the valence band.

The BIS results show a rather broad structure, indicating more than one final d electron addition state. Band theory predicts a dispersional width of the $3d$ band of only 1.5 eV, so this width must be due to the multiplet structure of the d^{n+1} ($\sim d^8$) state of Co due to both crystal fields and exchange, as discussed in detail below. The BIS spectra change somewhat on x even for $x \leq 0.2$, but again the biggest change is for $LiCoO_2$, where the BIS is nearly consistent with a single d electron addition state. This would be expected if Co in $LiCoO_2$ is trivalent and in a low-spin configuration [$d^6=(t_{2g})^6(e_g)^0$, $S=0$].

The Co_3O_4 results also show a single peak. The crystal structure of Co_3O_4 is a normal spinel structure.[44] On the tetrahedral sites we have Co^{2+} ions and on the octahe-

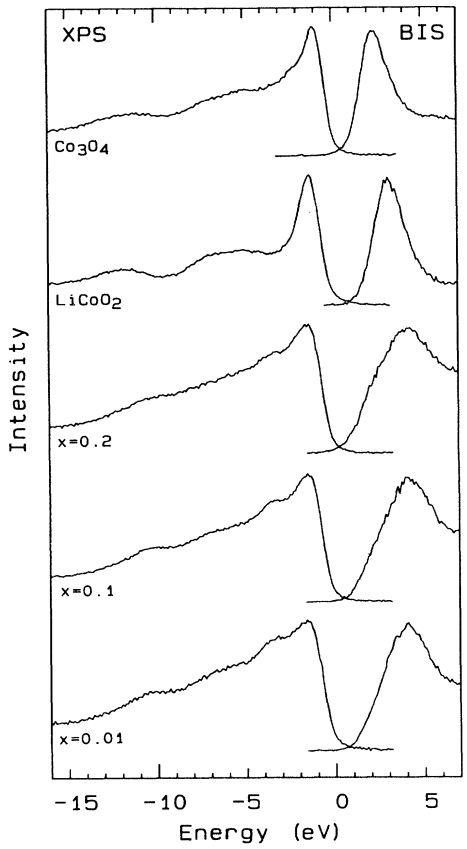

FIG. 5. XPS valence-band and BIS conduction-band measurements of $Li_xCo_{1-x}O$, $LiCoO_2$, and Co_3O_4.

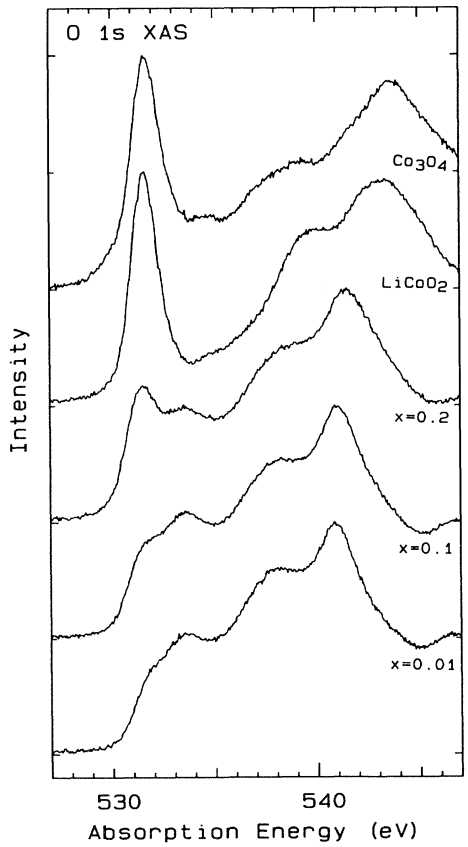

FIG. 4. O 1s XAS spectra of $Li_xCo_{1-x}O$, $LiCoO_2$, and Co_3O_4.

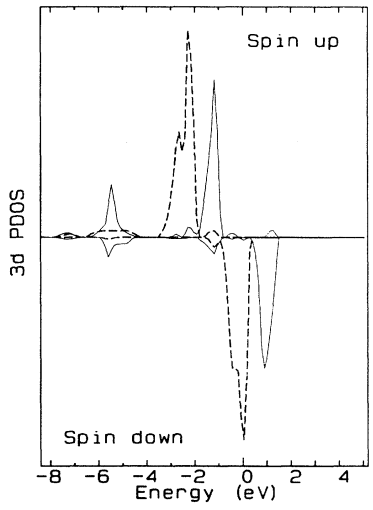

FIG. 6. Co $3d$ PDOS of CoO in the AFII ordering [taken from Ref. 43, Fig. 9(a)]. The solid (dashed) lines denote e_g (t_{2g}) contributions.

dral sites Co^{3+} ions. The tetrahedral sites have, compared to the octahedral sites, and inverted crystal-field splitting. Here the two e_g-symmetry orbitals are lower in energy than the three t_g-symmetry orbitals. Also, the splitting is smaller by a factor of $\frac{4}{9}$, so even for the short Co-O distance (1.929 Å for the tetrahedral site, 1.916 Å for octahedra) the Co^{2+} is high spin. The Co^{2+} can be written here as $d^7=|(e_g\uparrow)^2(t_{2g}\uparrow)^3(e_g\downarrow)^2\rangle$, with three empty minority-spin t_{2g} orbitals. The sharp conduction-band structure must be a result of the near degeneracy of the four empty e_g (Co^{3+}) and three t_{2g} (Co^{2+}) holes.

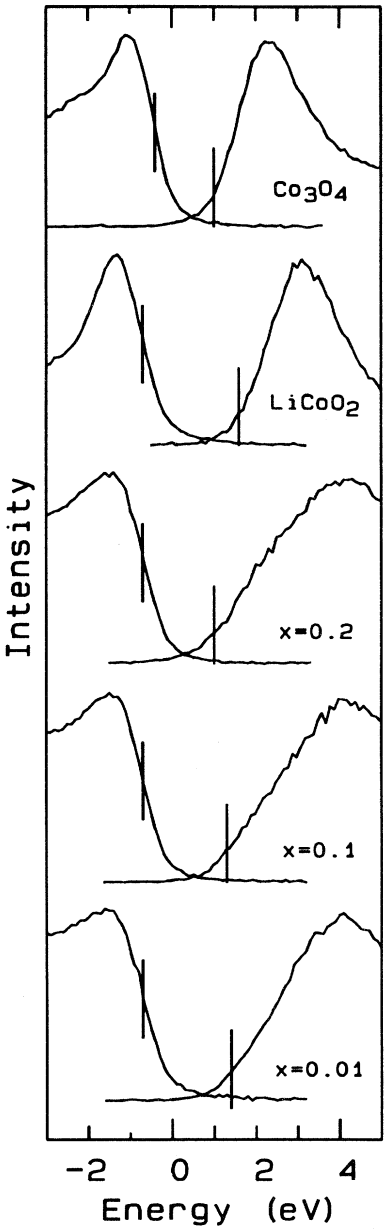

FIG. 7. The XPS and BIS spectra of Fig. 5 in a small-energy region. The vertical bars indicate the positions of the gap. For XPS this is taken at 50% of the intensity increase because the increase is equal to the used resolution (1.0 eV). In BIS we use a point at 10% intensity increase and add 0.4 eV, which is half of the BIS resolution as measured on a clean Cu sample in going from 10% to 90% intensity at threshold. The values of the gaps are listed in Table II.

A combination of XPS and BIS also yields quite clearly the band gap that is defined as the minimum energy required to remove an electron ($E_0^{n-1}-E_0^n$) plus the minimum energy required to add one ($E_0^{n+1}-E_0^n$). In Fig. 7 we show a smaller energy scale region of the XPS–BIS spectra in order to obtain the gap. The vertical lines indicate the position of the thresholds, taking into account an experimental broadening of 1.0 eV in XPS and 0.8 eV in BIS. The values of the gap are given in Table II. We see a closing of the gap with increasing x to 2.0 eV for $x=0.2$; however, $LiCoO_2$ has an even larger gap (2.7 eV) than CoO. The gap of Co_3O_4 is considerably smaller (1.6 eV).

The gap of 2.5 eV for CoO is at first glance inconsistent with optical-absorption data.[45,46] Upon comparing the optical data of Powell and Spicer[45] for CoO with that of NiO, it is observed that the midpoint of the strong rise in the CoO absorption edge occurs at an even higher energy than in NiO, indicating a gap of larger then 4 eV. In fact, Shen *et al.*[26] define a gap in this way of about 6 eV. However, the shape of the edge is quite different. The onset is much broader in CoO, indicating a smaller minimum gap with a weaker optical absorption. This is in fact clearly visible in the data of Pratt and Coelho,[46] where the absorption onset occurs between 2.5 and 3.0 eV. Since the first electron addition state in CoO is of t_{2g} character and the first electron removal state is of intermediate-spin character as we will show below with a strong O $2p$ component, the band-gap transition is expected to be optically weak. This is because the band-gap transition would involve removing a majority-spin e_g electron from the vicinity of one Co^{2+} ion and adding a minority-spin t_{2g} electron around a different Co^{2+} site. Spinwise this is allowed if the two sites are antiferromagnetically coupled. However, the optical transition matrix elements will be much smaller than if both of the states involved are strongly covalent e_g orbitals as in NiO.

To investigate the valence band of $LiCoO_2$ more extensively, we have also performed resonant photoemission (RPES) experiments near the Ni $3p$ edge at Daresbury (UK). The valence band as a function of the different photon energies is shown in Fig. 8. At 90-eV photon energy the valence band has the same overall structure as in the XPS spectrum. The cross-section ratio between Co $3d$ and O $2p$ decreases with decreasing photon energy.[47] The structure at 5 ± 2 eV is therefore strongly related to O $2p$ final states. At the photon resonance energy ($\sim$62 eV) we see a sharp antiresonance in the narrow line at 1.4 eV, indicating Co $3d$ final states. At the high-binding-energy satellite ($\sim$12 eV) we also find antiresonant behavior, as shown in Fig. 9, indicating Co $3d$ spectral weight in this area. In the $LiCoO_2$ cluster calculation part we will discuss these results by comparing it with the results of the

cluster calculation.

The qualitative conclusions reached from the experimental data are the following: (a) The local Co electronic structure is only weakly depending on Li doping up to $x=0.2$, but is quite different for $LiCoO_2$, for which the spectra indicate a low-spin Co^{3+} (d^6) configuration. (b) Oxygen 1*s* XAS data indicate a substantial change in the local conduction-band structure with Li substituton but no clearly separated Li-induced hole state is observed, as was the case in $Li_xNi_{1-x}O$.[18] (c) The valence- and conduction-band 3*d* spectral weight is distributed over a large energy scale, indicating strong electron correlation effects. (d) The band gap decreases somewhat with Li doping but then increases to an even larger value for $LiCoO_2$ than for CoO. (e) The Fermi level appears to be pinned at about 0.7 eV from the valence band for $0 \le x \le 0.2$. (f) Resonant photoemission experiments of $LiCoO_2$ show Co 3*d* related final states at the narrow line at 1.4 eV and spread out between 8 and 13 eV.

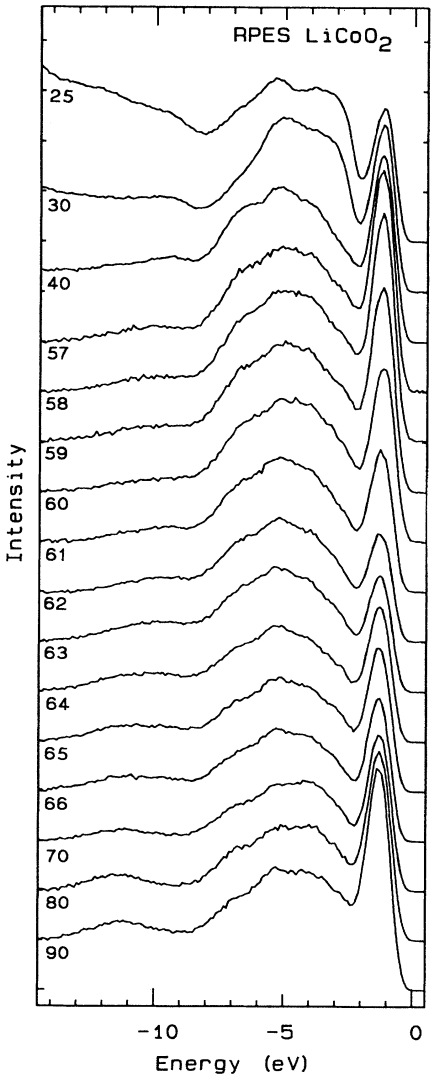

FIG. 8. Photon-dependent photoemission spectra of $LiCoO_2$. The different photon energies are listed in the figure.

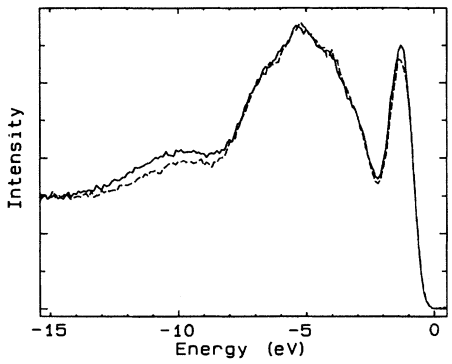

FIG. 9. Resonant photoemission spectra of $LiCoO_2$ with 63-eV (solid line) and 62-eV (dashed line) photon energy.

DISCUSSION

Before going into more-detailed calculations we will present a qualitative discussion of the results. The large satellite in the Co $2p^{3/2}$ XPS spectrum of CoO is reminiscent of NiO,[48] Ni dihalides,[49] and the Co dihalides.[37,38] A simple cluster model Hamiltonian calculation has been quite successful in describing these core-hole line shapes.[37,38,44] Recently more sophisticated calculations for divalent Cu oxides including also the multiplet structure have been able to clarify some finer details in the satellite line shapes.[50,51] These more-detailed calculations are not yet possible for Co^{2+} because of computer limitations, so we restrict ourselves to a more global discussion. In the simple model the ground state of CoO in a cluster with Co at the center is of the form

$$\psi_g = \alpha|d^7\rangle + \beta|d^8\underline{L}\rangle + \gamma|d^9\underline{L}^2\rangle \ , \tag{1}$$

where $\underline{L}$ represents an O 2*p* hole and the $d^{10}\underline{L}^3$ configuration has been neglected. The only local symmetry that needs to be considered here is the ${}^4T_{1g}$ state, since this is the Hunds-rule ground state of the high-spin Co^{2+} in an octahedral point group. Its electronic configuration is roughly $[(t_{2g}\uparrow)^3(e_g\uparrow)^2(t_{2g}\downarrow)^2]$. In the core-hole final state in the Co 2*p* XPS spectra the core-hole potential Q lowers the $d^8\underline{L}$ and $d^9\underline{L}^2$ states by Q and $2Q$ as compared to the d^7 state, causing a different ordering of levels, which is the reason for the strong satellite structure.[52] The situation for the O 1*s* XPS is quite different, since the O 1*s* core-hole potential will push up further the $d^8\underline{L}$ and $d^9\underline{L}^2$, therefore the lowest-energy state with an O 1*s* core hole present is similar to that of

the ground state and therefore little if any satellite structure is expected. This has been discussed in detail by Eskes and Sawatzky.[36] Another reason for a low O 1*s* satellite is that the oxygen 1*s*-2*p* Coulomb interaction of around 5–6 eV is, compared to the oxygen bandwidth, not large enough to pull out local bound states. The $\underline{L}$ states are spread out over four to six neighboring oxygen atoms, so if a bound state is not pulled out the effective influence of the core hole is only 1–1.5 eV. In Fig. 10 we show the energy levels and the changes that occur upon introducing the Co 2*p* core hole for XPS and XAS. We see from Fig. 10 that if $Q > \Delta$, the first two energy levels in the XPS final states are inverted as compared to the ground state, and this results in a large satellite.[49] Since in general $U \sim 0.7Q$, this also means that U must be comparable to Δ. If we look at a general analysis of the Co 2*p* core lines by Oh and Park *et al.*,[37,38] $U \sim \Delta$ is found.

From Fig. 10 it is also clear why the Co 2*p* XAS spectra do not have large satellites. The final core-hole states upon the addition of a *d* electron are $\underline{c}d^8$ and $\underline{c}d^9\underline{L}$, which have the same ordering in the ground state, so that all the intensity is in the lowest-energy state. Another way of saying this is that the extra *d* electron almost perfectly screens the core hole. This is also the reason why the Co 2*p* XAS shows the multiplet structure characteristic of that for a free ion in a cubic crystal field. Indeed, the so-renormalized free-ion theoretical spectrum calculated by de Groot *et al.*[40] for $10Dq \sim 1$ eV is very close to that observed for CoO in Fig. 3.

Before going on to a detailed cluster calculation for the CoO and $LiCoO_2$ valence- and conduction-band structure, we present arguments as to why $LiCoO_2$ has a low-spin rather than a high-spin ground state, and what the nature of the charge compensating state in $Li_xCo_{1-x}O$ is. That $LiCoO_2$ is indeed low spin is very clear, first of all from a comparison of the Co 2*p* XAS spectra (Fig. 3) with the calculation of Co^{3+} low spin as shown by de Groot *et al.*,[40] and second in the sharp empty 3*d* structure measured with BIS and O 1*s* XAS. To understand this, consider first the simple crystal-field type of picture of the filling of the *d* states as a function of $10Dq$, as shown in Fig. 11 for Co^{3+} (d^6). For the free ion the majority- and minority-spin states are split by $J_{\text{eff}} = 31B + 10C - 2(193B^2 + 8BC + 4C^2)^{1/2}$. At a $10Dq$ value corresponding to the dashed line, a high-spin to low-spin transition takes place. This occurs for $10Dq > 2.1$ eV in the XAS calculations of de Groot *et al.*[40] In CoO, Co^{2+} is high spin, and as we substitute Li up to $x = 0.2$ it keeps the characteristic features of high-spin Co^{2+}. However, as in Li-doped NiO we are decreasing the number of states in the σ antibonding O 2*p* – Co 3*d* hybridized orbitals, so the lattice parameter will decrease because of a decreased Born repulsion between O 2*p* and Co 3*d*. The decreases in lattice parameter for both $Li_xCo_{1-x}O$ and $Li_xNi_{1-x}O$ are shown in Fig. 12. We see a smooth decrease in lattice parameter in the NiO system, but for the CoO system the ordered $LiCoO_2$ phase has a much smaller Co-O distance than that extrapolated from the $x \leq 0.2$ behavior. We note that there is a miscibility gap for $0.2 < x < 0.5$. Since a smaller CoO distance increases the O 2*p* – Co 3*d* transfer integral T_{pd}, it also increases the ligand field contribution to $10Dq$. When a sufficiently high $10Dq$ is reached to be almost in the low-spin configuration, it becomes advantageous to further empty the e_g orbitals so that the Co-O distance can decrease further with a subsequent catastrophic increase in T_{pd} and eventually a low-spin ground state. This causes an avalanche kind of effect.

A reasonable estimate of the change in T_{pd} in going from CoO to $LiCoO_2$ can be made using Harrison's relations[53] $T_{pd} \sim 1/r^{3.5}$, from which $T_{pd}(LiCoO_2) \sim 1.44T_{pd}(CoO)$. The ligand field splitting is, from perturbation, given by

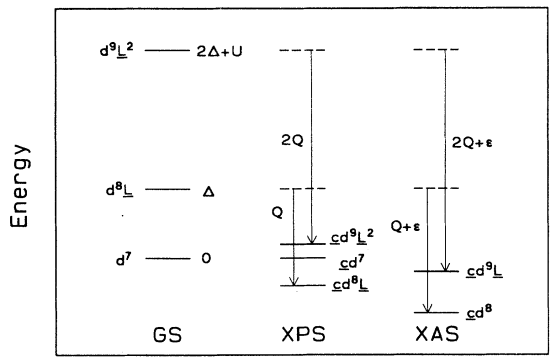

FIG. 10. Energy-level scheme without a core hole (GS) in the presence of a core hole (XPS), and in the presence of a core hole and an extra 3*d* electron (XAS). The energy difference between $\underline{c}d^8\underline{L}$ (XPS) and $\underline{c}d^8$ (XAS) is the ligand ionization potential ε.

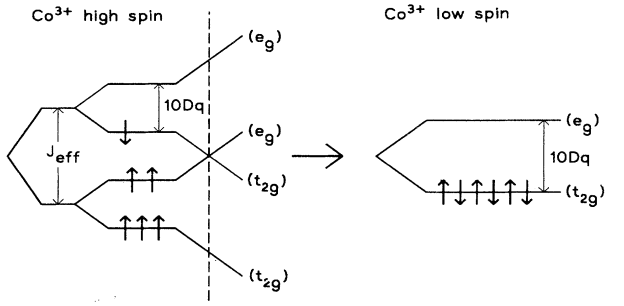

FIG. 11. The change in ordering of the Co^{3+} *d* orbitals in going from high spin (left) to low spin (right). In the high spin (left) we have an ordering with the first five spins up split by the ligand field into t_{2g} and e_g orbitals and one spin down in a t_{2g} orbital. The majority- and minority-spin states are split by a Hunds-rule exchange J_{eff}. In going to low-spin Co^{3+} the ligand field splitting increases and at the dashed vertical line the majority-spin e_g and minority-spin t_{2g} orbitals cross. The result is the low-spin Co^{3+} (right) with $(t_{2g})^6$ where now the spin-up and spin-down states are degenerate.

$$10Dq \simeq \frac{T_{pd\sigma}^2}{\Delta} - \frac{T_{pd\pi}^2}{\Delta} \simeq \frac{3T_{pd\sigma}^2}{4\Delta} . \quad (2)$$

We define $T_{pd\sigma}=\sqrt{3}(pd\sigma)$ (the Slater-Koster transfer integrals)[54] and take $T_{pd\sigma}\simeq 0.5T_{pd\pi}$.[53] Therefore we expect an increase in $10Dq$ by about a factor of 2, which certainly is enough to stabilize the low-spin state.

Because of the large spectroscopic differences between $Li_xCo_{1-x}O$ and $LiCoO_2$, it is not realistic to assume that the charge compensating states in $Li_xCo_{1-x}O$ are of Co^{3+} low-spin nature. In the BIS we see mainly empty Co $3d$ states. In the oxygen $1s$ XAS we probe the empty O $2p$ states directly and see a much stronger effect here. This means that the extra holes have a large amount of oxygen character. To explain this we have to look at different oxygen-hole symmetries possible and the different hybridization strengths. The most important configurations for the Li-doped case consist of d^6 and $d^7\underline{L}$ states. These states are almost degenerate, since, as we will show below and expect from estimated values,[20,21] $U\sim\Delta$. To find the lowest-energy state we must consider the various symmetries and spin states of relatively low energy. These are $(t_{2g}\uparrow)^3(e_g\uparrow)^2(t_{2g}\downarrow)^1$ with high-spin $S=2$ and $(t_{2g}\uparrow)^3(e_g\uparrow)^1(t_{2g}\downarrow)^2$ with intermediate-spin $S=1$ for d^6 and for $d^7\underline{L}$ $(t_{2g}\uparrow)^3(e_g\uparrow)^2(t_{2g}\downarrow)^2\underline{L}(t_{2g}\downarrow)$ with $S=2$ and $(t_{2g}\uparrow)^3(e_g\uparrow)^2(t_{2g}\downarrow)^2\underline{L}(e_g\uparrow)$ with $S=1$. Of the two $d^7\underline{L}$ states the one with the ligand hole in an e_g orbital is the lowest in energy because of O-O transfer integrals. It is stabilized by $2(pp\sigma-pp\pi)$ relative to the $\underline{L}(t_{2g})$ state. The states of d^6 and $d^7\underline{L}$ of the same spin and symmetry hybridize with different strengths depending on σ- or π-bonding oxygen orbital combinations, resulting in an energy-level diagram as shown in Fig. 13. So in $Li_xCo_{1-x}O$ we can expect to find that induced hole states are antiferromagnetically coupled with the Co^{2+}, giving an intermediate-spin $S=1$ state. The induced holes have considerable oxygen character. The $S=1$ spin state gives a decreased magnetic moment of the Co ion, as is found in susceptibility measurements.[14]

The forming of low-spin Co^{3+} for Li substitution above $x=0.2$ is probably the reason for the miscibility gap in $Li_xCo_{1-x}O$ for $x>0.2$. The U value in CoO is given approximately by $U=A+B$, where the Racah A parameter is screened from the free-ion value down to about 5.2 eV (see below). This screening is, as shown by de Boer, Haas, and Sawatzky,[55] mainly due to the polarizability of O^{2-}, and increases with decreasing Co-O distance as $1/r^3$, so A in $LiCoO_2$ is expected to be smaller. It is more difficult to estimate what happens to Δ because Δ is proportional to the Madelung potential, which will increase with decreasing Co-O distance but will decrease because of the increasing covalency, especially in the low-spin ground state. Because of the large T_{pd} value for $LiCoO_2$, we expect the ground state to be strongly covalent. The experimental gap of 2.7 eV puts lower bounds on U and Δ.

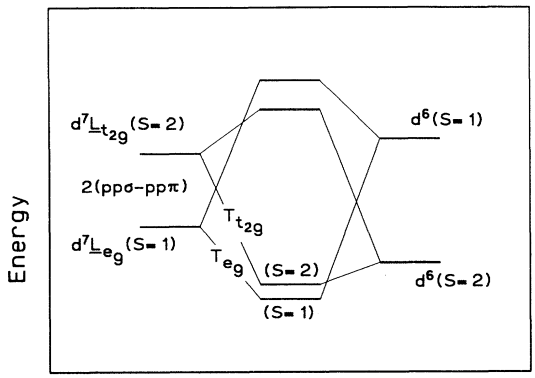

FIG. 13. An artist's impression of the Li-doped strongly covalent ground state of "Co^{3+}." On the left the extra hole has entered into oxygen states and on the right it has entered a Co d orbital. In the middle we see the effect of the strong hybridization for the σ bonding extra e_g hole, making the intermediate spin state $S=1$ lowest in energy. The $d^7\underline{L}$ and d^6 states are nearly degenerate in CoO because $U\sim\Delta$.

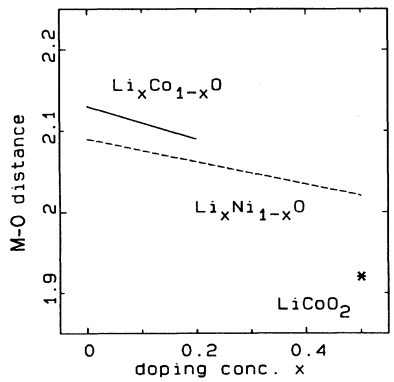

FIG. 12. The transition-metal oxygen distance of $Li_xCo_{1-x}O$, $Li_xNi_{1-x}O$, and $LiCoO_2$.

MODEL HAMILTONIAN CLUSTER CALCULATIONS

To determine values for the various interactions discussed above, we compare the experimental spectra to the results of a cluster calculation. The aim of the cluster calculation is to obtain (a) the CoO $3d$ electron removal spectral weight, to be compared with the CoO valence-band XPS; (b) the character (symmetry, spin, and orbital composition) of the first ionization state of CoO; (c) the CoO $3d$ electron addition spectral weight, to be compared with the measured CoO conduction band; (d) the $LiCoO_2$ electron removal and addition spectral weight, to be compared with the XPS and BIS data on $LiCoO_2$. The model calculations use a CoO_6 cluster in octahedral symmetry. The model Hamiltonian is given by

$$\mathbf{H}=\mathbf{H}_0+\mathbf{H}_1 , \quad (3)$$

$$\mathbf{H}_0=\sum_m E_d(m)d_m^\dagger d_m+\sum_m E_p(m)p_m^\dagger p_m+\sum_m T_{pd}(m)(d_m^\dagger p_m+p_m^\dagger d_m)\ , \tag{4}$$

$$\mathbf{H}_1=\sum_{m,m',n,n'} U(m,m',n,n')d_m^\dagger d_{m'}d_n^\dagger d_{n'}\ . \tag{5}$$

The indices m,m',n,n' denote orbital and spin quantum numbers. We include all the Co $3d$ orbitals but only the oxygen orbital combinations that can hybridize with the Co $3d$ orbitals. As a "vacuum" for CoO we take the Co^{2+} (d^7) Hunds-rule ground state (^4F as a free ion) and a closed oxygen $2p$ shell. The operator $d_m^\dagger$ creates a Co $3d$ hole with energy $E_d(m)$. We have included an ionic point-charge crystal-field splitting $10Dq^{(i)}$, which splits the $3d$ orbital energies into a doubly degenerate e_g level at $E_d(e_g)=E_d-6Dq^{(i)}$ and a triply degenerate level at $E_d(t_{2g})=E_d+4Dq^{(i)}$. The value used in CoO for $10Dq^{(i)}$ ($=0.7$ eV) is equal to a value found in an impurity calculation[21] and a cluster calculation[56] of the optical spectrum of NiO and is consistent with the experimental data.

The operator $p_m^\dagger$ creates an O $2p$ hole with energy $E_p(m)$. The ligand hole wave functions consist of linear combinations of oxygen $2p$ orbitals with the appropriate (d orbital) symmetries. The Slater-Koster[54] oxygen nearest-neighbor interactions $(pp\sigma)$ and $(pp\pi)$ split the oxygen states into a doubly degenerate state with e_g symmetry at $E_p(e_g)=E_p-[(pp\sigma)-(pp\pi)]$ and a triply degenerate state with t_{2g} symmetry at $E_p(t_{2g})=E_p+[(pp\sigma)-(pp\pi)]$. The value of $(pp\sigma)-(pp\pi)$ for CoO is governed by the width of the oxygen band in CoO (~ 4 eV). These values are 60% larger then those found by Mattheiss,[57] who used a nonorthogonal basis.

The last term of $\mathbf{H}_0$ describes the one-particle hybridization between the Co $3d$ states and the ligand orbitals. T_{pd} is the transfer integral for Co $3d$–O $2p$ hybridization. This is written in terms of Slater-Koster[54] $(pd\sigma)$ and $(pd\pi)$ transfer integrals. We define Δ as the energy needed in the ground state for removing an electron from O $2p$ to the Co $3d$ empty states ($\Delta=E_p-E_d$).

$\mathbf{H}_1$ describes the two-particle $3d$ Coulomb and exchange interactions U. The calculation includes the d-d Coulomb and exchange interactions using the full atomic multiplet theory as fully specified in terms of the Racah A, B, and C parameters. For CoO the B and C parameters of the unscreened atomic values of Co^{2+} are taken as tabulated by Griffith.[58]

In this Hamiltonian we have neglected the Co $4s,4p$ levels and the empty O bands. These levels are assumed to be at high energy, so that their influence through hybridization can be treated as a renormalization of the effective parameters. We also neglect the O-O Coulomb interaction.

To reduce the size of the problem in the calculation of the ground state (three holes) of CoO we omit the $d^{10}\underline{L}^3$ states. This hardly influences the results because they are high in energy. In the electron removal spectrum we omit for the same reason the $d^{10}\underline{L}^4$ states. The many-body Hamiltonian is solved exactly by means of a continued-fraction expansion of the Green's function, giving directly the electron removal or addition spectra.

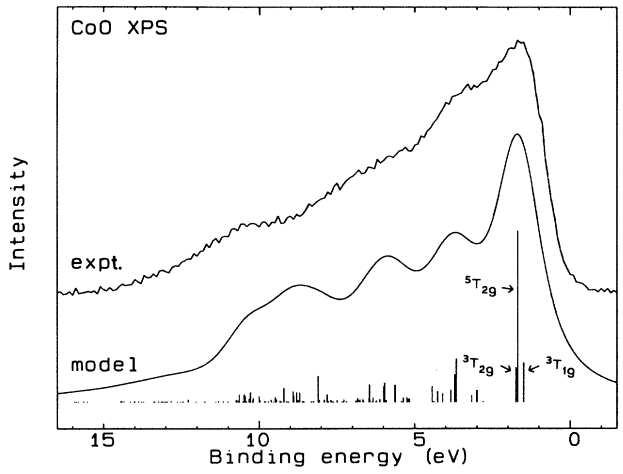

FIG. 14. The XPS valence band of CoO (top) as compared with the Co $3d$ removal spectral weight of the CoO_6 cluster calculation (bottom). The vertical lines indicate the energy positions and intensities of the CoO final states. Taking the Co $3d$–O $2p$ cross sections (Ref. 47) into account we should add about 6% oxygen spectral weight around 4-eV binding energy. The parameters are listed in Table III.

For the actual calculation of the CoO $3d$ removal spectral weight we treat three parameters as free variables. These are the cobalt to oxygen charge-transfer energy Δ, the Racah A parameter responsible for the d-d Coulomb interaction, and the Co-O hybridization $(pd\sigma)$. The transfer integral $(pd\pi)$ is taken to be $-0.45(pd\sigma)$.[57] The parameters are obtained with the following criteria from the CoO data: (a) the spectral weight must be spread over 10 eV; (b) the intensity has to go down continuously from low binding energy to high binding energy, with about 25% left at the highest satellite binding energy; and (c) there must be a gap of more than 3 eV, to take the translational invariance into account. The gap is determined (if Δ is larger then A) by the Racah A pa-

TABLE III. The model parameter values used in the CoO_6 cluster calculation for CoO and $LiCoO_2$.

		CoO (eV)	$LiCoO_2$ (eV)
Racah	A	5.2	5.0
	B	0.14	0.15
	C	0.54	0.60
Δ		5.5	4.0
$(pd\sigma)$		1.3	1.9
$(pd\pi)$		−0.6	−0.9
$(pp\sigma)$		0.55	0.65
$(pp\pi)$		−0.15	−0.20
$10Dq^{(i)}$		0.7	1.0
U		5.3	3.5
E_{gap}		3.1	3.5

rameter, the charge-transfer energy Δ as compared to the Racah A parameter, and T_{pd} determines the intensity slope. We find $0 \leq \Delta - A \leq 0.5$ eV. The calculation shown in Fig. 14 is for $A = 5.2$ eV, $\Delta = 5.5$ eV, and $(pd\sigma) = 1.3 \pm 0.1$ eV. All the parameters are listed in Table III. The cross-section ratio for Co $3d$ compared to O $2p$ is 15.4,[47] so the oxygen spectral weight is expected to be about 6% of the total Co $3d$ electron removal spectral weight. The oxygen band intensity would be expected to be around 4±2-eV binding energy. Taking this into account, our fit to the experimental CoO valence band is now quite satisfactory.

The first ionization state in CoO is expected to be the charge compensation state on doping with Li and is therefore of considerable importance. With the same parameters the first ionization state is of $^3T_{1g}$ character, an intermediate-spin state as predicted by the simple considerations above. The next ionization state is of $^5T_{2g}$ character and the third is of $^3T_{2g}$ character. Table IV shows the occupation numbers and main wave functions of the ground state and the first two ionization states. We see that the first two ionization states have considerable $d^7\underline{L}$ character.

To investigate the stability of the intermediate spin state $^3T_{1g}$ as the first ionization state, we investigated the influence of the Co $3d$–O $2p$, hybridization, the neglect of U_{pp}, and a change in $\Delta - A$ on the energy difference between the $^3T_{1g}$ and the $^5T_{2g}$ symmetry states. The energy difference is found to increase linearly with increasing cobalt oxygen hybridization, changing from 0 for $(pd\sigma) = 1$ to 0.4 for $(pd\sigma) = 1.6$ eV. We see a strong influence of the hybridization, but on broad range of $(pd\sigma)$ values the $^3T_{1g}$ states will be the first ionization state.

The influence of the $d^8\underline{L}^2$ states through hybridization on the final states is considerable because of its energy position $(2\Delta - U)$ above d^6. This means that the neglect of the O-O Coulomb interaction U_{pp} can influence the nature of the first ionization state considerably. The holes of the $\underline{L}^2$ state, however, can avoid each other because we have six oxygen neighbors, so in only one in six cases do we expect to raise the $d^8\underline{L}^2$ energy level with U_{pp}. We can estimate the influence by raising the entire $d^8\underline{L}^2$ level as compared to the d^6 and $d^7\underline{L}$ levels through the simultaneous increase of A and Δ by $U_{pp}/6$ (~ 1 eV). This reduces the difference between the intermediate and the high spin to 0.10 eV. For A and Δ raised with 2 eV we find degenerate levels. An increase of $\Delta - A$ is found, as expected, to influence the energy difference between the $^3T_{1g}$ and $^5T_{2g}$ symmetry states considerably. For $\Delta - A = 1.0$ eV these symmetry states are degenerate.

TABLE IV. Occupation numbers of the ground state and the first two ionization states of CoO.

Ground state		Ionization states	$^3T_{1g}$	$^5T_{2g}$
d^7	0.79	d^6	0.19	0.36
$d^8\underline{L}$	0.20	$d^7\underline{L}$	0.62	0.53
$d^9\underline{L}^2$	0.01	$d^8\underline{L}^2$	0.18	0.11
		$d^9\underline{L}^3$	0.01	0.00

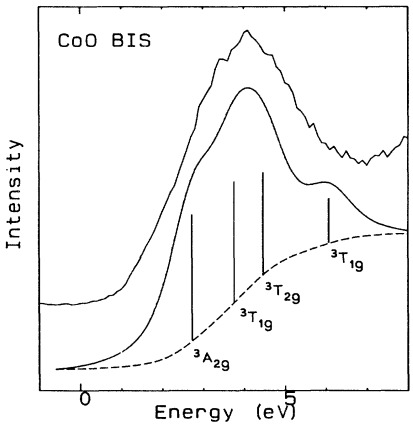

FIG. 15. The CoO BIS spectrum (top) compared with the BIS cluster results (bottom solid line). The bottom dashed line is a background added to the calculation. The vertical lines indicate the energy positions and intensities of the d^8 final states. For the parameters used see Table III, and for the positions, intensities, and symmetries see Table V.

For the standard parameter set of CoO we can also calculate the electron addition spectral weight (Fig. 15). We find four states with the symmetries $^3A_{2g}$, $^3T_{1g}$, $^3T_{2g}$, and $^3T_{1g}$, respectively. As noted above, a simple ligand field picture of CoO would yield only two levels corresponding to the addition of a t_{2g} or e_g electron. The first three states come from the $^3F(d^8)$ free-ion multiplet. We can compare the electron addition spectrum with the measured conduction band (see Fig. 15). To do this we added to the calculated spectrum a background proportional to the integrated intensity. We see that the cluster calculation can explain the broad conduction-band structure very well.

The calculated CoO spectrum depends very strongly

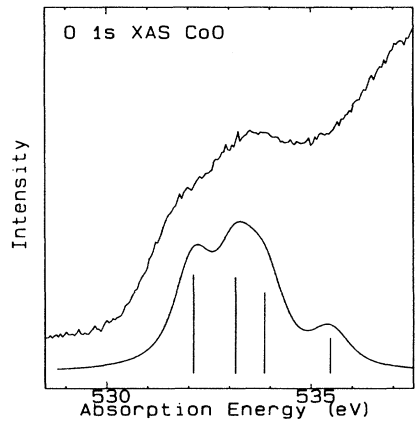

FIG. 16. The CoO O 1s XAS spectrum (top) compared with the BIS cluster results. The vertical lines indicate the energy position and intensity of the d^8 final states.

on the value of the point-charge $10Dq^{(i)}$ parameter. The $d^9\underline{L}$ final states are $U+\Delta$ ($\sim$10 eV) above the d^8 final states. So the hybridization and the form of the oxygen band have little influence on the splittings, as do small changes in U and Δ. To show that the point-charge crystal-field parameter $10Dq^{(i)}$ is a necessity, we also calculated the spectral weight for $10Dq^{(i)}=0$ eV, and find almost no splitting of the t_{2g} and e_g states (see Table V). The energy difference between the first three symmetries comes now only from the hybridization with the $d^9\underline{L}$ final states at $U+\Delta$. This hybridization is smaller than in the ground state, leading to small ligand field splittings.

If we neglect the O 1s core-hole potential, then the states reached by O 1s XAS are the same as those reached in BIS, although the relative intensities can be quite different. The O 1s XAS spectrum shown in Fig. 16 indeed shows a pre-edge structure consisting of at least two components. The vertical bars indicate the positions of the calculated BIS states, yielding the correct energy spread.

Using the same model Hamiltonian parameters of CoO, we also calculated the energies of the d-d optical transitions from the ground state of CoO. If we compare our calculated values (see Table VI) with the optical-absorption spectrum measured by Pratt and Coelho (Fig. 1, Ref. 46), we find the agreement to be satisfactory, also in view of the simplified nature of the model Hamiltonian. This is also a confirmation of the value taken for the point-charge contribution to the crystal field of 0.7 eV.

For the cluster calculation on the Co^{3+} low spin of $LiCoO_2$ in a CoO_6 cluster we use some adjustments to our parameter set. According to Harrison,[53] the oxygen nearest-neighbor interactions $(pp\sigma)$ and $(pp\pi)$ will increase as $1/r^2$. This means an increase of 20% in the oxygen bandwidth; $(pp\sigma)-(pp\pi)$ is changed from 0.7 eV in CoO to 0.85 eV here. Racah B and C parameters for Co^{3+} are not tabulated, so we used Co^{2+} values[58] increased by about 10%. This increase is generally found in the 3d, transition metals in going to higher oxidation states.

The definitions of U and Δ for the low-spin Co^{3+} are basically the same as for Co^{2+} in CoO. Δ is defined as the energy needed to remove an electron from the full oxygen orbitals to an empty Co 3d orbital, but now with a d^6 vacuum state. U is defined here as the energy needed for transferring a 3d electron to another Co^{3+} ion. These are not the Hunds-rule lowest-energy multiplets for d^5, d^6, and d^7, but these are the multiplets ^2D, ^1S, and ^2D for d^5, d^6, and d^7, respectively, consistent with a low-spin d^6 state.

In the calculation of the $LiCoO_2$ we can treat the same three parameters as free variables. But we can get an impression about the value of $(pd\sigma)$ by using Harrison's relations,[53] as was done before. This indicates a $(pd\sigma)$ value of around 1.8 eV. As reported above, the cross-section ratio for Co 3d compared to O 2p is 15.4.[47] In $LiCoO_2$ this changes because we have one fewer 3d electron and the number of oxygens is doubled. Now we have to add 15% oxygen spectral weight to our cluster calculation.

In the actual calculation we therefore use the following criteria: (a) the high-binding-energy satellite at 12-eV binding energy should be reproduced at the correct position and with the correct intensity; (b) a gap of more than 3 eV to take the translational invariance into account. In Table III we list the parameters used, and in Fig. 17 we show our calculated 3d removal spectral weight and the experimental XPS valence band. From the calculation it is quite clear that the broad structure around 5-eV binding energy has a lot of oxygen character. If we add here about 15% spectral weight the actual fit is quite satisfactory. We used $(pd\sigma)=1.9$ eV, slightly larger than predicted. To get the low-spin ground state we had to in-

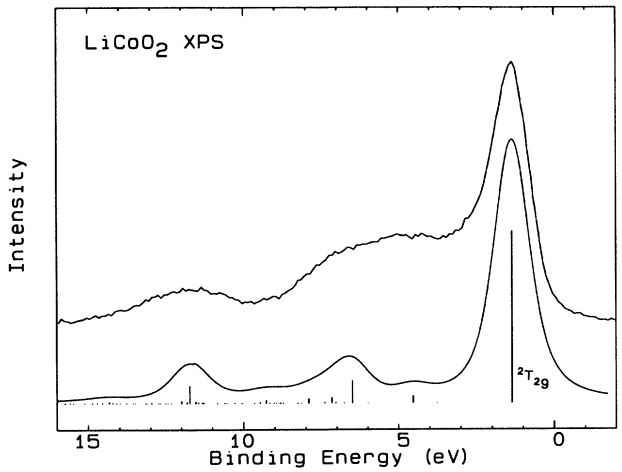

FIG. 17. The XPS valence band of $LiCoO_2$ (top) as compared to the Co 3d removal spectral weight of the cluster calculation with low-spin Co^{3+} (bottom). The vertical lines indicate the energy positions and intensities of the XPS final states. Around 5±2-eV binding energy one should, at about 15% of the Co 3d spectral weight, take photoemission from the oxygen 2p states into account.

TABLE V. Energies, intensities, and symmetry of the CoO d^8 final states reached in BIS. Energies are in eV.

	$10Dq=0.7$		$10Dq=0$	
Symmetry	Energy	Intensity	Energy	Intensity
$^3A_{2g}$	0.00	0.310	0.0	0.293
$^3T_{1g}$	+1.03	0.308	+0.35	0.293
$^3T_{2g}$	+1.73	0.258	+0.62	0.219
$^3T_{1g}$	+3.08	0.111	+2.42	0.171

TABLE VI. Energy and symmetries of the calculated d-d optical forbidden absorptions in CoO using the parameters of Table III. Energies are in eV.

Energy position		
Theory	Expt.	Symmetry
0.73	0.74	^2E_g
	0.92	
1.07	1.03	$^4T_{2g}$
1.92	2.04	$^2T_{1g}$
2.46	2.32	$^2T_{2g}$
2.68	2.5	$^4T_{1g}$
3.06		$^4A_{2g}$

crease the crystal-field parameter $10Dq^{(i)}$ to $10Dq^{(i)}=1.0$ eV. This must be a consequence of the smaller Co-O distance.

The distribution of the $3d$ spectral weight and the calculated value for the gap are not very sensitive to changes in A and Δ. This is a result of the large hybridization. The ground state is of very mixed character and consists of 47% d^6, 44% $d^7\underline{L}$, and 9% $d^8\underline{L}^2$, yielding a strongly covalent bonding in $LiCoO_2$. The first ionization state and first electron addition state are also of very mixed character (see Table VII). The first electron addition state is one sharp state, as is seen in BIS. In the resonant photoemission experiment of $LiCoO_2$ we found Co $3d$ spectral weight resonating at the main line and at high binding energy (8–13 eV). These are exactly the positions where in the cluster calculation the $3d$ electron removal spectral weight is found. One is tempted to use RPES to distinguish between d^n and $d^{n+1}\underline{L}$ final states.[59] This can only be easily done for d^9 initial states as for Cu^{2+} compounds.[60] The problem is further complicated by the following process, which should also be taken into account ($\underline{c}$ stands for the Co $3p$ core hole):

$$(t_{2g}\uparrow)^3(t_{2g}\downarrow)^3\rightarrow\underline{c}(t_{2g}\uparrow)^3(t_{2g}\downarrow)^3(e_g\uparrow)^1$$
$$\rightarrow(t_{2g}\uparrow)^3(t_{2g}\downarrow)^1(e_g\uparrow)^1+e\ . \qquad (6)$$

Now we have a final state with $S=\frac{3}{2}$, a state not reached in the photoemission process because it would involve a spin change of $\frac{3}{2}$. The interpretation of the resonant photoemission experiment for Co compounds is therefore extremely complicated but also very interesting.

Since U and Δ are comparable, one might expect the d^5 and $d^6\underline{L}$ states in the ionized $LiCoO_2$ to be nearly degenerate, whereas a splitting in these of about 10 eV is observed (see Fig. 17). This very large "satellite" energy is due primarily to the large p-d hybridization. One must realize that for a configuration like t_{2g}^5 there are four empty e_g orbitals to hybridize with full O $2p$ σ-bonding orbitals. Taking these four to be degenerate, the effective matrix element coupling $d^5(t_{2g}^5)$ and $d^6(t_{2g}^5e_g^1)\underline{L}$ is $\sqrt{4}[\sqrt{3}(pd\sigma)]\cong 5.3$ eV according to Table III. So degenerate states would split up by 10.6 eV, as observed. This is a good example of how satellite positions are dominated by hybridization effects rather than U and Δ.

If we compare the parameters of CoO with $LiCoO_2$, the main difference is the hybridization parameter $(pd\sigma)$. From the values of $U\sim\Delta$ in CoO we would expect a Δ for $LiCoO_2$ of $U-\Delta\sim 0$ eV if there were no changes in crystal structure, Madelung potential, or lattice parameters. However, we find in $LiCoO_2$ the first charge-transfer state still about 4 eV above the d^6 level. The covalency of $LiCoO_2$ is therefore a consequence of the strong hybridization.

CONCLUSIONS

We have investigated the electronic structure of CoO and have found that CoO is a highly correlated insulator. We found a gap of 2.5 ± 0.3 eV, which is smaller than that found in NiO. By the use of a model cluster calculation we find that the first ionization state in CoO is of $^3T_{1g}$ symmetry, corresponding to an intermediate-spin state. The charge of the extra hole is to a large extent on the O $2p$ states. On doping with holes this is expected to be the charge compensating state. The stability of this state is investigated, and a change of hybridization and the neglect of the O-O Coulomb interaction does not change the symmetry of this first ionization state. The stability of this state as compared to the $^5T_{2g}$ high-spin state is, however, strongly dependent on the energy difference $\Delta-A$. We find for the Mott-Hubbard U a value $U=5.3$ eV ($U=A+B$) and for the charge transfer energy Δ a value of $\Delta=5.5$ eV. This places CoO in the intermediate region of the ZSA diagram.[22] The spread of the electron addition states of CoO as measured with BIS and oxygen $1s$ XAS can be well explained by the use of the cluster calculation. The point-charge crystal-field splitting of the Co $3d$ orbitals is responsible for the energy spread in these states, as the cluster calculation shows. The other parameters have only a small influence on the calculated spectral weight.

TABLE VII. Occupation numbers of the ground state and electron removal ($^2T_{2g}$) and addition (^2E_g) final states of $LiCoO_2$.

GS		Removal		Addition	
d^6	0.47	d^5	0.17	d^7	0.77
$d^7\underline{L}$	0.44	$d^6\underline{L}$	0.51	$d^8\underline{L}$	0.22
$d\underline{L}^2$	0.09	$d^7\underline{L}^2$	0.29	$d^9\underline{L}^2$	0.01
$d^9\underline{L}^3$	0.00	$d^8\underline{L}^3$	0.03		

Upon substitution of Co with Li in $Li_xCo_{1-x}O$, the compensating holes reside primarily in O $2p$ states and are most likely bound to nearest-neighbor Li impurity sites for $x\leq 0.2$. The band gap does not close, staying at about 2.0 eV for $x=0.2$. The impurity potential therefore seems to be at least 1 eV. The O $2p$ holes are strongly hybridized with neighbor Co $3d$ states resulting in a large antiferromagnetic exchange interaction and a resulting magnetic moment that looks like that of Co^{3+} intermediate spin.

In $LiCoO_2$, the end member of Li doping, the situation is quite different. We find low-spin Co^{3+} responsible for and stabilized by the small Co-O distance found experimentally. The fingerprint of low-spin Co^{3+} is clearly visible in the used spectroscopies. We find a gap of 2.7 ± 0.3 eV. The cluster calculation of $LiCoO_2$ shows a strongly mixed ground state, making $LiCoO_2$ strongly covalent. The valence-band photoemission experiments can be satisfactorily explained by the cluster calculation.

The electronic structure of Co_3O_4 is well understood with the Co^{2+} on tetrahedral and low-spin Co^{3+} on the octahedral positions in the normal spinel lattice. The gap is found to be 1.6 ± 0.3 eV.

ACKNOWLEDGMENTS

This work was supported by the Netherlands Foundation for Fundamental Research on Matter (FOM), the Netherlands Foundation for Chemical Research (SON), and the Netherlands Organization for the Advancement of Pure Research (NWO).

[1]H. J. de Boer and E. J. W. Verwey, Proc. Phys. Soc. London, Ser. A **49**, 59 (1937).
[2]A. H. Wilson, Proc. R. Soc. London, Ser. A **133**, 458 (1931).
[3]F. Bloch, Z. Phys. **57**, 545 (1929).
[4]J. G. Bednorz and K. A. Muller, Z. Phys. B **64**, 189 (1986).
[5]N. F. Mott, Proc. Phys. Soc. London, Ser. A **62**, 416 (1949).
[6]J. Hubbard, Proc. R. Soc. London, Ser. A **277**, 237 (1964); **281**, 401 (1964).
[7]C. R. Ronda, G. J. Arends, and C. Haas, Phys. Rev. B **35**, 4038 (1987).
[8]A. Fujimori and F. Minami, Phys. Rev. B **30**, 957 (1984).
[9]G. A. Sawatzky and J. W. Allen, Phys. Rev. Lett. **53**, 2339 (1984).
[10]J. Ghysen, L. H. Tjeng, J. van Elp, H. Eskes, J. Westerink, G. A. Sawatzky, and M. T. Czyzyk, Phys. Rev. B **38**, 11 322 (1988).
[11]Z. X. Shen, J. W. Allen, J. J. Yeh, J. S. Kang, W. Ellis, W. E. Spicer, I. Lindau, M. B. Maple, Y. D. Dalichaouch, M. S. Torikachvili, J. Z. Sun, and T. H. Geballe, Phys. Rev. B **36**, 8414 (1987).
[12]A. Fujimori, E. Takayama-Muromachi, Y. Uchida, and B. Okai, Phys. Rev. B **35**, 8814 (1987).
[13]R. R. Heikes and W. D. Johnston, J. Chem. Phys. **26**, 582 (1957).
[14]W. D. Johnston, R. R. Heikes, and D. Sestrich, J. Phys. Chem. Solids **7**, 1 (1958).
[15]A. J. Bosman and C. Crevecoeur, J. Phys. Chem. Solids **30**, 1151 (1969).
[16]A. J. Bosman and A. J. van Daal, Adv. Phys. **19**, 1 (1970).
[17]K. Mizushima, P. C. Jones, P. J. Wiseman, and J. B. Goodenough, Solid State Ion. **3/4**, 171 (1981).
[18]P. Kuiper, G. Kruizinga, J. Ghysen, G. A. Sawatzky, and H. Verweij, Phys. Rev. Lett. **62**, 221, (1989).
[19]J. van Elp *et al.* (unpublished).
[20]J. Zaanen and G. A. Sawatzky, J. Solid State Chem. **88**, 8 (1990).
[21]J. Zaanen, Ph.D. thesis, University of Groningen, The Netherlands, 1986.
[22]J. Zaanen, G. A. Sawatzky, and J. W. Allen, Phys. Rev. Lett. **55**, 418 (1985).
[23]K. S. Kim, Phys. Rev. B **11**, 2177 (1975).
[24]M. Oku and K. Hirokawa, J. Electron Spectrosc. **8**, 475 (1976).
[25]M. Oku, J. Solid State Chem. **23**, 177 (1978).
[26]Z. X. Shen, J. W. Allen, P. A. P. Lindberg, D. S. Dessau, B. O. Wells, A. Borg, W. Ellis, J. S. Kang. S. J. Oh, I. Lindau, and W. E. Spicer, Phys. Rev. B **42**, 1817 (1990).
[27]Z. X. Shen, C. K. Shih, O. Jepson, W. E. Spicer, I. Lindau, and J. W. Allen, Phys. Rev. Lett. **64**, 2442 (1990).
[28]Janet L. Mackay and V. E. Heinrich, Phys. Rev. B **39**, 6156 (1989).
[29]N. B. Brookes, D. S. Law, D. R. Warburton, P. L. Wincott, and G. Thorton, J. Phys. Condens. Matter **1**, 4267 (1989).
[30]H. J. Orman and P. J. Wiseman, Acta Crystallogr. C **40**, 12 (1984).
[31]N. K. Appandairajan, B. Viswanathan, and J. Gopalakrishnan, J. Solid State Chem. **40**, 117 (1981).
[32]H. Peterson, Nucl. Instrum. Methods Phys. Res. A **246**, 260 (1986).
[33]J. Fink, Th. Muller-Heinzerling, B. Scheerer, W. Speier, F. U. Hillebrecht, J. C. Fuggle, J. Zaanen, and G. A. Sawatzky, Phys. Rev. B **32**, 4899 (1985).
[34]C. T. Chen and F. Sette, Rev. Sci. Instrum. **60**, 1616 (1989).
[35]F. M. F. de Groot *et al.* (unpublished).
[36]H. Eskes and G. A. Sawatzky, Phys. Rev. B **43**, 119 (1991).
[37]S. J. Oh, in *Core-Level Spectroscopy in Condensed Systems,* edited by J. Kanamori and A. Kotani (Springer-Verlag, New York, 1988).
[38]J. Park, S. Ryu, M. Han, and S. J. Oh, Phys. Rev. B **37**, 10 867 (1988).
[39]P. F. Bongers, Ph.D. thesis, University of Leiden, The Netherlands, 1957 (unpublished).
[40]F. M. F. de Groot, J. C. Fuggle, B. T. Thole, and G. A. Sawatzky, Phys. Rev. B **42**, 5459 (1990).
[41]M. Grioni, M T. Czyzyk, F. M. F. de Groot, J. C. Fuggle, and B. E. Watts, Phys. Rev. B **39**, 4886 (1989).
[42]F. M. F. de Groot, M. Grioni, J. C. Fuggle, J. Ghijsen, G. A. Sawatzky, and H. Peterson, Phys. Rev. B **40**, 5715 (1989).
[43]K. Terakura, T. Oguchi, A. R. Williams, and J. Kuebler, Phys. Rev. B **30**, 4734 (1984).
[44]W. L. Roth, J. Phys. Chem. Solids **25**, 1 (1964).
[45]R. J. Powell and W. E. Spicer, Phys. Rev. B **2**, 2182 (1970).
[46]G. W. Pratt and R. Coelho, Phys. Rev. **116**, 281 (1959).
[47]J. J. Yeh and I. Lindau, At. Data Nucl. Data Tables **32**, 1 (1985).
[48]S. Hüfner, Solid State Commun. **49**, 1117 (1984).
[49]J. Zaanen, C. Westra, and G. A. Sawatzky, Phys. Rev. B **33**, 8060 (1986).
[50]K. Okada and A. Kotani, J. Phys. Soc. Jpn. **58**, 2578 (1989).
[51]K. Okada and A. Kotani, J. Electron. Spectrosc. Relat. Phenom. **52**, 313 (1990).
[52]G. A. Sawatzky, in *Solid State Chemistry 1982, Proceedings of the 2nd European Conference, Veldhoven, The Netherlands, 1982,* edited by R. Metselaar, H. J. M. Heijligers, and J. Schoonman, Studies in Inorganic Chemistry Vol. 3 (Elsevier, Amsterdam, 1983).
[53]W. A. Harrison, *Electronic Structure and the Properties of Solids* (Freeman, San Francisco, 1980).
[54]J. C. Slater and G. F. Koster, Phys. Rev. **94**, 1498 (1954).
[55]D. K. G. de Boer, C. Haas, and G. A. Sawatzky, Phys. Rev. B **29**, 4401 (1984).
[56]J. van Elp (unpublished).
[57]L. F. Mattheiss, Phys. Rev. B **5**, 290 (1972).
[58]J. S. Griffith, *The Theory of Transition Metal Ions* (Cambridge University Press, Cambridge, 1961).
[59]L. C. Davis and L. A. Feldkamp, Phys. Rev. B **23**, 6239 (1981).
[60]J. Ghijsen, L. H. Tjeng, H. Eskes, G. A. Sawatzky, and R. L. Johnson, Phys. Rev. B **42**, 2268 (1990).